An approach for data-driven characterization of tide and current fluxes in coastal basins

Elvira Armenio[1], Francesca De Serio[1], Michele Mossa[1]

[1]Department of Civil, Environmental, Building Engineering and Chemistry, Technical University of Bari, Bari, 70125, Italy

Correspondence to: Elvira Armenio (elvira.armenio@poliba.it)

Abstract. Recently, much effort has been spent in the attempt to provide predictions of physical processes at coastal sites. Numerical models are more and more adopted to characterize hydrodynamics and sediment transport features and their use is encouraged because of their feasible applicability, accuracy and cost. In any way, they need for parameters calibration and validation of results, thus requiring a sensitivity analysis and increasing in turn the demand for rich and comprehensive sets of data. Our work aims to demonstrate that a data approach, besides supporting and improving numerical modelling, has also an additional advantage, i.e. allows to directly identify the key physical processes driving a coastal system as well as to assess their relative strength under diverse conditions. This is especially true in restricted coastal environments, where numerical models could fail because of small spatial scales and fine temporal resolution. In the present case, we illustrate and analyse a unique data set comprising a sequence of detailed measurements of tides, waves and 3D currents, continuously acquired each hour at the same time and location for three months. Evidence of recurring patterns and cycles was inferred, thus showing the possibility to extrapolate these data also in a forecasting perspective. Our method is based on (i) the analysis of temporal trends and variability of hourly-averaged vertical profiles of the current velocity for a variety of tidal conditions; (ii) the spectral analyses of tide levels and water currents measured at different depths; (iii) the computation of the tidal asymmetry factor; and (iv) the harmonic analysis of the tidal constituents. Consequently, details on the vertical structure of the flow, on the correlation between currents and tide, on the tidal asymmetry as well as on flood or ebb dominance are the principal outcomes of this study. Our data approach and results are documented through the detailed study of the Mar Piccolo, a shallow water basin located in the inner part of the Ionian Sea (Southern Italy). While the type of coherent patterns observed are site-specific, the approach and investigation framework are general and may be employed in diverse settings.

1 Introduction

A thorough knowledge of the hydrodynamic conditions is generally the basis of any study in coastal environment, and in the framework of management plans and decision-making. Most of the numerical models used in predictive operational oceanography allow to reproduce and predict these hydrodynamic processes, taking into account regional, sub-regional and coastal scales. On the contrary, they do not reach spatial resolutions lower than a few hundred meters (Samaras et al., 2016). Consequently, difficulties are encountered when typical features of coastal engineering should be studied at local scale. Reliable modelling systems that can scale down from the ocean to the coastal scale have emerged as a need and the recent tendency is to develop multiscale modelling systems, based on a multiple-nesting approach (Samaras et al., 2016). To provide reliable results and enhance their predictive capabilities, all these models have to face two heavy limitations: i) they need to be calibrated and validated by means of waves, current and tide measurements (De Serio et al. 2007; De Serio and Mossa, 2014); ii) the accuracy of model outputs relies on the quantity, quality and duration of the available observations.

Usually one of the most basic problems encountered in coastal datasets is the poor resolution in time of data, which are often intermittent or too sparsely sampled. Spatial sampling is generally guaranteed with surveys along fixed transects at regular intervals (Reeve et al., 2016), but in general these surveys are made on ad hoc monitoring programs, with time duration of a few days. Furthermore, both monitoring campaigns and installation of fixed sensors are generally time consuming and expensive and become logistically challenging especially in semi enclosed areas or in very shallow coastal waters, where it is difficult to assess field data. Consequently, even if strongly necessary, field measurements are still rare or incomplete (De Serio et al., 2015; Sauvageta et al., 2000; Benque´at al., 1982), so that monitoring actions should be rationally programmed.

In any case, it is worth noting that field information of high quality, i.e. simultaneous measurements derived by continuous and long term monitoring, above all near the coastline, are fundamental not only with the aim to estimate the most suitable modelling system or to allow numerical models tuning, running and validating. In fact, an approach based on historical data collections also allows to identify some patterns and physical processes established in the site during a certain temporal interval, without necessarily turning to mathematical modelling.

Obviously, the data approach has significance only if applied to continuous data, assessed for a sufficiently long time frame, with a proper sampling frequency, in order to capture seasonal or even annual typical features in the investigated site and also on small spatial scales. Moreover, the data approach enables to find evidence of recurring trends and cycles in the investigated site. Consequently, when recurring patterns emerge from an observational work, they can be extrapolated and used for practical predictions, provided that no changes occur in the settled configuration. If the investigated scenario is subjected to modifications, extrapolating trends is possible only if such changes have been captured in the measurement records. Otherwise, forecasts should be preferred as a product of numerical modelling.

From these brief notes, having at disposal a large amount of high quality hydrodynamic data seems essential to improve the understanding of many coastal phenomena. Specifically, the continuous monitoring of tides, waves and currents in a nearshore region is fundamental to understand the role that they play in coastal processes, morphodynamic changes and pollution spreading, even more in restricted coastal settings, such as bays, lagoon, estuaries and semi-enclosed basin. As an example, these coastal environments may be tidally dominated and consequently characterized by horizontal movements of sea water accompanying the rising and falling of the tide. Additionally, some peaks of current velocities may be observed along the tidal cycle in conjunction with a tidal asymmetry, i.e. when the inequality in the ebb and flood durations occurs. It is also worth noting that flood/ebb tidal dominance plays a pivotal role in the estuarine sediment transport and morphodynamics (Brown and Davies, 2007), as it is likely to control the direction and magnitude of net landward or seaward sediment fluxes and hence sediment accretion or erosion. As well, it is worth remembering that pollutant fate and dispersion processes are strictly connected to currents and waves propagation (De Serio and Mossa, 2016a; 2016b).

The data-driven approach here adopted involves: (i) a preliminary inspection executed on the assessed data with the spectral analysis, allowing to filter out spurious signals; (ii) the analysis of temporal trends and variability of hourly-averaged vertical profiles of the current, extracted for selected phases along the tidal period; (iii) the spectral analyses of tide levels and water currents measured at different depths, in order to find possible correlations; (iv) the computation of the tidal asymmetry factor and (v) the harmonic analysis of the tidal constituents, to identify spatial and/or temporal asymmetry and flood or ebb dominance. These processing methodologies are classical, well-established and not demanding in computational terms. Thus, they can be easily employed in different settings. We illustrate the application of the data approach to a target area in Southern Italy, considered highly vulnerable, being exposed to heavy urban and industrial pressure. Consequently, its safeguard is one of the main aims of the local environmental policy. Therefore, a

continuous monitoring action of the principal hydrodynamic parameters in this site, by means of proper sensors, is considered a useful managing tool, in terms of planning and prevention along with intervention when some accidental spills occur. The hydrodynamic circulation in this area has been investigated in literature generally by means of numerical modelling and mainly considering the system as governed by the wind and the tidal forcing (De Serio et al., 2007;

5   Scroccaro et al., 2004; Umgiesser et al., 2007). Still few studies (De Serio and Mossa, 2015; 2016a; 2016b) have started to examine large on site datasets, but they concerned above all the area outside the basin. The present study examines novel data assessed in a monitoring station close to the inner basin. The investigated period refers to the last autumn-winter season (01.10.2015 ÷ 31.12.2015), due to the start-up and working properly of the measuring system.

The paper is structured as follows. In section 2 the target site and the adopted procedures to measure and process data are

10   described. Section 3 displays the principal findings of the study and Section 4 discusses about possible data correlation and recurring trends.

2 Materials and methods

2.1 Study site and data sources

The proposed approach is applied to a target area, i.e. a shallow water basin named Mar Piccolo and located in the inner

15   part of the Ionian Sea (Fig.1a). It is composed by two bays, respectively named I Bay and II Bay. Its total surface is about 21.7 km^2, its maximum depth is around 15m in the I Bay and 10m in the II Bay (De Serio and Mossa, 2016b; De Pascalis et al., 2015). It is joined to Mar Grande, an external basin, by means of an artificial channel, i.e., the Navigable Channel, and a natural one, i.e., the Porta Napoli Channel (Fig.1b). The Navigable Channel is 58m wide, 375m length and 14m deep, while the Porta Napoli Channel is 150m wide and 2.5m depth. With regards to these dimensions, its hydrodynamic

20   patterns could be properly studied only on a local scale.

During May 2014, a monitoring station was installed in the Navigable Channel (Fig. 1). The geographical coordinates of Station *A* are 40.473° N and 17.235° E and its local depth is on average 13.7m. The station is equipped with a bottom mounted ADCP and a wave array, both by Teledyne RD. The acoustic frequency of the ADCP is 600KHz and the velocity accuracy is 0.3% of the water velocity ±0.003m/s. The ADCP is bottom mounted, upward facing and has a pressure sensor

25   for measuring mean water depth. The transducer head is at 0.50m above the seafloor. Velocities are sampled along the water column with 0.50 m vertical bin resolution and a 1.60 m blanking distance. The water column is therefore investigated from a distance from the sea bottom of 2.1m up to the most superficial bin not biased by waves. The surface layer, with a thickness on average equal to 1.5 m, is excluded from the analysis.

Starting from June 2014, mean current velocity profiles have been collected continuously at 1 hour intervals, using an

30   average of 60 measurements acquired every 10s. In this way, hourly averaged velocity components along the water column are provided. Analogously, hourly values of significant wave height *Hs* have been acquired.

On August 2015, an ultrasonic tide gauge (by General Acoustics) was settled in the Navigable Channel at Station *B* (Figure 1b). It is a stand-alone water level gauge, whose probe records and calculates the time that an acoustic pulse employs to be reflected vertically on the sea surface. The ultrasonic tide gauge is installed on a swinging bridge crossing

35   the Channel, named S. Francesco di Paola. Starting from September 2015, hourly values of tide levels have been acquiring with a sampling rate of 5Hz, while the gauge accuracy is ±0.01m.

In addition, five accelerometer sensors were considered in the present analysis. The sampling rate of these sensors was 1000Hz and they were placed in the centreline of the bridge S. Francesco di Paola.

2.2 Data processing

Available scalar and vector data were managed in the way further detailed.

A preliminary evaluation of the reliability of data recorded by the ultrasonic tide gauge was carried out with the spectral analysis. To evaluate the possible correlations between the measured currents flowing in the channel and the tidal records, the vertical profiles of current velocities were extracted for selected phases along the tidal period. The Fast Fourier Transform (FFT) algorithm was used to relate tidal and current data at different water depth. Successivly, the tidal asymmetry was analysed applying two different approaches to identify spatial and/or temporal asymmetry and flood or ebb dominance. Finally, considering that in shallow coastal waters and tidal inlets energy from the dominant fundamental tidal constituents is non-linearly transferred through processes including advection, finite-amplitude effects and friction, generating higher harmonic overtides and compound tides, a harmonic analysis was conducted on the tidal signal (Aubrey and Speer, 1985; Speer and Aubrey, 1985; Di Lorenzo, 1988; van de Kreeke, 1988; Westerink et al., 1988; Le Provost, 1991; Fortunato and Oliveira, 2004). In this way, the relationship between the *M2* (astronomical constituent) and the *M4* (shallow-water constituent) amplitude and phase, commonly used in identifying the nature of the tide or tidal current asymmetry, was investigated (Boon and Byrne, 1981; Friedrichs and Aubrey, 1988).

2.2.1 Analysis of recorded tide and wave data

Tidal data were first examined to assess the reliability of the used ultrasonic tide gauge in Station *B*. Once blanks were removed, the data were checked and were promptly compared with the tide levels recorded at Station St. Eligio (Fig. 1) and managed by the national tide gauge network of the Italian Institute for Environmental Protection and Research (ISPRA). The time frame used as reference period was $01.10.2015 \div 31.12.2015$. Station St. Eligio is located outside the Mar Piccolo at geographical coordinates 40° 28 '32.17"*N* and 17° 13' 25.55"*E* at a distance of about 700m from Station *B* (Fig. 1).

Firstly, the FFT technique was applied to process the tidal data recorded from both Station *B* and Station St. Eligio, thus allowing a comparison of their amplitude spectra in the frequency domain. Successively, a further analysis was carried out, considering that for technical reason the ultrasonic tide gauge is set on the swinging bridge crossing the Navigable Channel, subjected to intense and heavy road traffic. The traffic-induced vibrations should not influence the tide gauge measurements, since the tidal record and bridge vibration frequencies are expected to be in completely different ranges. Nevertheless, since the gauge metallic support is clamped to the bridge structure, possible displacements could be amplified, inducing some disturbances on the tidal signal as a consequence. Therefore, in a cautionary perspective, an analysis of the tidal and bridge vibration signals was carried out in the frequency domain. The bridge vibrations were investigated by processing the field data provided from five accelerometer sensors installed on the bridge and available for the day 08.10.2012. Two data sets were examined, referring to a duration time of 300 seconds each. The first spanned a time window from 12:54 a.m. to 12:59 a.m. and the second from 03.06 p.m. to 03:11 p.m. These two samples were taken into account because respectively representative of an intense and a light traffic condition.

The time series of the acceleration records were processed by means of a double numerical integration using the trapezoid method. With this procedure, the time series of the bridge vibrations were computed.

For completeness, the time series of the measured significant wave heights H_s acquired in Station *B*, provided with a wave meter and a processed by a module for real-time collection of hourly wave data, were also examined for the same reference time window.

2.2.2 Analysis of recorded sea current data

The hourly-averaged vertical profiles of the current velocities recorded in Station A of the Navigable Channel (Fig. 1b) were analysed for the reference period, displaying trends which highlight a variable structure of the flow along the water depth.

5 For the successive analysis, the current velocities in the horizontal plane, originally measured along E-W and N-S directions respectively, were managed by a plane rotation of the coordinate system, to get their components along the transversal and longitudinal channel axis, which is 12° clockwise rotated from N (Fig. 2). Conventionally, the longitudinal velocity components v are positive if entering towards the Mar Piccolo, while the transversal velocity components u are positive if directed to the eastern bank of the channel.

10 Based on the available topographic data, the cross section of the Navigable Channel was deduced and the net flows through the Navigable Channel were estimated for the investigated period, considering that the transversal u velocities could be disregarded in this computation. In this way, it was approximated that the flow was uniform along the longitudinal axis of the channel. The monthly-averaged longitudinal current velocities were evaluated for each depth cell of the ADCP and multiplied by the corresponding sub-section of the channel itself.

15 ### 2.2.3. Analysis of recorded tide

Firstly, it was considered that in the entrance to a bay or strait (as for the case of the Navigable Channel), the tidal current is reversing, i.e. it flows alternately in approximately opposite directions with an instant or short period of little or no current, called slack water, occurring at each reversal. During the flow in each direction, the current velocity varies from zero, at the time of slack water, to a maximum, called flood or ebb, about midway between the slacks (Brown et al., 2007; 20 Dronkers, 1998; Dronkers, 1986). To investigate on the reversing tidal current in the Navigable Channel, the time series of the tide was overlapped to the time series of the longitudinal current velocity at various depths.

Successively, the asymmetry of the tidal current was examined. This is a common phenomenon in tidal inlets and plays an important role in sediment transport processes and pollutions spreading within the inlet. Tidal asymmetry can be flood or ebb dominant and it can be spatial and/or temporal (Dronkers, 1986). Flood dominant asymmetry occurs when the 25 flood current is stronger than the ebb current, while ebb dominant asymmetry occurs in the opposite situation (Jewell et al., 2015, Nidzieko, 2010). As indicator of ebb or flood dominance, the ratio R of peak ebb current and peak flood current was computed for the present case and for the reference period. Consequently, the ebb dominance condition is characterized by $R \geq 1$, on the contrary, the flood dominance condition by $R \leq 1$. To investigate on the tidal spatial asymmetry, i.e. on the tidal asymmetry near the bottom, at intermediate depth and at the surface, the ratio R was computed 30 at the investigated depths, for two consecutive ebb and flood currents.

Also the inequality in the temporal durations of successive ebb and flood phases was considered as a further condition to identify temporal asymmetry. Tidal asymmetry was thus indicated by a disparity between the number of ebb and flood current hours in the time series.

The application of a tidal asymmetry factor γ proposed by Dronkers (1998) was also used as an additional approach to 35 investigate on tidal asymmetry. Referring to the study conducted by Townend (2005), Townend et al. (2000), Friedrichs and Aubrey (1988) and Aubrey and Speer (1985) for different inlets and estuaries with a triangular cross-section shape, it was demonstrated that the tidal asymmetry factor can be expressed as:

5

$$\gamma \propto \left[\frac{h+a}{h-a}\right]^2 \frac{S_{LW}}{S_{HW}} \approx \left(1 + 2\frac{a}{h}\right)\left(\frac{\frac{v_c}{h}\left(1-\frac{a}{h}\right)}{\frac{v_c+v_s}{h}+\frac{a}{a}}\right) + O\left(\frac{a}{h}\right)^2 = \frac{\left(1+\frac{a}{h}\right)}{\left(1+\frac{\frac{v_c}{v_s}}{\frac{a}{h}}\right)} \tag{1}$$

where a is the amplitude of the tidal range, h is the mean depth, v_s is the volume of the intertidal storage (i.e. the volume between low water and high water over intertidal areas), v_c is the volume of the channel (i.e. the volume of the channel

5 delimited by the mean tide level), S_{LW} and S_{HW} are the surface at low and high tide, respectively.

A value of γ equal to one suggests a uniform tide characterized by equal duration of ebb and flood currents, so that the tide is symmetrical. The condition $\gamma >1$ results in flood-asymmetry (long slow ebb and short fast flood), while the condition $\gamma < 1$ results in ebb-asymmetry (long slow flood and short fast ebb).

To have a further confirmation of the abovementioned results, the least-squares harmonic analysis of the signal acquired

10 in Station B was computed, using the Matlab T_Tide package (Pawlowicz et al., 2002). The results from the harmonic analyses were used to investigate the relation between the various shallow-water tidal constituents that might contribute to tidal asymmetry. The tidal regime in the study area was furtherly identified by the evaluation of form number F, defined by Pugh (1987) as

15 $F = \frac{O_1+K_1}{M_2+S_2}$, $\tag{2}$

where O1 is the principal lunar diurnal, K1 is the lunisolar diurnal, M2 is the principal lunar semidiurnal and K2 is the principal solar semidiurnal. Considering eq. (2), the condition $0.25 \leq F < 1.5$ represents a mixed primarily semidiurnal tide characterized by two high and two low waters each tidal day, with relatively small differences in the respective highs

20 and lows.

In tidal inlets where semi-diurnal tides prevail, the dominant offshore forcing tide is the principal semi-diurnal lunar $M2$ tidal constituent, as in our case. The type of tidal asymmetry can be characterized by phase and amplitude relations between the $M2$ tide and its first harmonic, the shallow water $M4$ constituent (Boon and Byrne, 1981; Aubrey and Speer, 1985; Boon, 1988; Di Lorenzo, 1988; Friedrichs and Aubrey, 1988; Moore et al., 2009).

25 Aubrey and Speer (1985) showed that the phase difference, $2\theta_{M2} - \theta_{M4}$ where θ is the phase of the tidal height, determines whether an inlet is flood dominated or ebb dominated. A 90° phase difference of tidal height means shorter flood duration (compared with ebb duration). This results in a higher flood current velocity and consequently a flood dominant situation. A 270° phase difference of tidal height means longer flood duration, which can result in a higher ebb current velocity than flood current velocity. Aubrey and Speer (1985) and Friedrichs and Aubrey (1988) conducted

30 theoretical studies and fieldwork on tidal asymmetry for estuaries with semidiurnal tidal regime. Based on their studies, under a semidiurnal regime, an inlet has flood-dominant current if $0° < 2\theta_{M2} - \theta_{M4} < 180°$ and ebb-dominant current if $180° < 2\theta_{M2} - \theta_{M4} < 360°$.

3. Results

3.1 Tide and waves

35 The time series of tide levels assessed at Station B and Station St.Eligio show that the target area is characterized by a semidiurnal tide. The maximum tide level recorded in the investigated period at Station B was 0.45m, while the minimum

was -0.25m. Applying the FFT algorithm, a general agreement is found between the two signals, which show the same peaks of amplitude at periods of 12h and 24h (Fig. 3a). The two data sets were also examined focusing on an extreme meteorological event, occurred on 16th October 2015, when during a storm the rainfall reached 0.191m in the city of Taranto in few hours during the morning. The time series of both Stations (Fig. 3b) display very similar trends of the recorded tidal levels, except than in a short time window (around 12:30 am), when consistently the outflow from Mar Piccolo flowing through the Navigable Channel increased due to the rainfall contribution, thus inducing a depth in Station B higher (about twice) than in Station St. Eligio. This behaviour highlights the trend of Mar Piccolo to act as a sort of catchment basin.

From the analysis of bridge vibration, for the sake of brevity, referring to one of the five accelerometer sensors, Figure 4a shows the time series of the calculated vibrations in the case of intense traffic condition. Similar trends and values were detected also referring to the other accelerometers. Measured accelerations are in the range 12-16m/s^2 and the deduced vibrations are less than 10^{-3}m in all cases. Using the FFT algorithm, the amplitude spectra of the bridge vibrations were obtained (Fig. 4b). The highest amplitudes are found in the frequency range of 2-2.5Hz as evident from the enlargement of Figure 4c. A prompt comparison of the amplitude spectra of tide level (Fig. 3a) and bridge vibrations (Fig. 4c) proves experimentally the expected results, i.e. the frequencies typical of the two signals are in different ranges, without any overlap.

Figure 5 shows the time series of the significant wave heights in the investigated period. The greatest value of observed H_s is equal to 0.8m, while the average value of H_s is around 0.3m. These values are consistent with the H_s data recorded in Mar Grande and shown in Armenio et al. (2016), which showed for the same season a maximum value around 1.2m. In fact, we could expect that swell waves, entering the Mar Grande basin from its *SW* opening (Fig.1), propagate throughout finally reaching the Navigable channel, where they arrive quite smoothed. The directions of the wave propagation in the Navigable Channel is generally confined to *NNE/SSW* due to the orientation of the Channel itself (clockwise rotated of ~12° from *N*).

3.2 Currents

Figure 6 shows a stick plot of the hourly measured currents at z=-2.0m, z=-5.5m and z=-10.5m respectively, being z the vertical distance from the sea surface. It is evident that the current is mainly oriented along the N-S axis, driven by the longitudinal direction of the channel, at all the investigated depths. From the stick plot of Figure 6, it is evident that the longitudinal current components are greater than the transversal ones, thus disregarded in the following analysis.

The values of the longitudinal velocity components v due to an inflow towards the Mar Piccolo are plotted in Figure 7a, once monthly-averaged in the reference period of measurement. The incoming flow is characterized by velocities spanning from 0.2m/s at surface layers to 0.15m/s near the bottom. Smaller values (v around 0.12m/s) are observed near the surface for the month of November. Figure 7b displays the monthly-averaged velocities of the outflow from the Mar Piccolo, with absolute values greatest in the most superficial layers (v around -0.25m/s), then decreasing while approaching the bottom (v around -0.12m/s). The transversal current components u varies in the range -0.08m/s÷0.023m/s, being one order of magnitude smaller than the longitudinal ones, as expected because of the restraint action played by the channel banks. Figure 8 illustrates the net flow across the Navigable Channel in the reference period, with positive sign referring to net flow entering toward the Mar Piccolo. At deeper layers, from the bottom up to z=-4m the net flow results inflowing, while in the most superficial layer it is directed outward of the basin. This resulting net flow agrees with a previous numerical modelling (De Pascalis et al., 2015), which represented the annual hydrodynamic simulation in this

site for the year 2013. Also, the annual field data by Armenio et al. (2016) and De Serio and Mossa (2015; 2016a) are consistent with these findings. In the abovementioned studies, a double circulation was observed in the Channel, characterized by an annual-averaged predominant outflow in the superficial layer and on the contrary an annual-averaged predominant inflow near the bottom.

3.3 Tide reversing and asymmetry

To investigate on the reversing tidal current in the Navigable Channel, the time series of the tide was overlapped to the time series of the longitudinal current velocity at various depths. Specifically, we observed that during each tidal cycle, the trend of the current at different depths showed recurring features. Therefore, the phase averages of both tide elevation and current velocity were computed and are plotted in Figure 9, referring to surface (z=-2m, z=-3.5m), intermediate (z=-6.5m) and bottom layers (z=-10.5m). The use of the phase averaging procedure assured that the observed behaviour is recurrent and Figure 9 can be considered representative of the investigated period. In Figure 9 the current flood peak in the surface layer (z=-2.0m) occurs at the same time of the high tide. At lower layers (z=-3.5m, z =-6.5m and z=-10.5m), there is a time lag of about two hours between the high tide and the flood current peak. In addition, it can be noticed a double-peaks flood current in the most superficial layers (z=-2.0m and z=-3.5m). This trend confirms the observation of Byun and Cho (2006) for the case of a semidiurnal tide dominated basin.

If all the water in the Mar Piccolo was in dynamic equilibrium with the external Mar Grande, the current would be zero (slack waters) when the tidal level inverts, i.e. at low and high tides. Figure 9 shows that, on the contrary, slack waters occur during the passage from high tide to low tide and vice-versa. Analysing the relationship between the instant times of high/low tide and the instant times of slack waters, the result is a progressive wave current. This means that the maximum flood and ebb occurs around the times of high and low tides, while slack waters occur in between. From the observed data, there is about a two-three hours lag between the time of slack waters and the low or high tide levels.

The findings about the tidal spatial asymmetry, i.e. on the tidal asymmetry near the bottom, at intermediate depth and at the surface, are summed up in Figure 10, where five examples representative of the trend in the reference period are illustrated, for the sake of brevity. In all the selected frames, at bottom layers $R \leq 1$ meaning flood stronger than ebb currents, on the contrary, at surface layers $R \geq 1$ meaning ebb stronger than flood current.

The tidal temporal asymmetry was also deduced, observing that the value of R varies in time at each water depth. As an example, Figure 11 shows the variability of R, computed as the ratio between the minimum and maximum current value for each day, referring to surface and bottom layers in the month of November 2015. Again, a predominance of flood currents in deeper layers is noted, with prevailing values of R<1, as well as a predominance of ebb currents in surface layers is obtained, with prevailing values of R>1.

The inequality in the temporal durations of successive ebb and flood phases showed that the number of ebb currents hours is greater than that of flood currents at surface layers. In particular, long and stronger ebb and short and slower flood currents were identified. On the contrary, at bottom layers, flood currents duration prevails over ebb currents duration. In particular, long and stronger flood currents with short and fast ebb currents were detected. At intermediate depths, comparable duration of flood and ebb currents was found. For the sake of brevity, Figure 12 shows, as an example, the temporal duration of flood and ebb currents at z=-2.0m, z=-6.0m and z=-11.5m for a selected short period.

The tidal asymmetry factor γ was also computed following eq. (1). A trapezoidal cross section with 25° sloped lateral sides was assumed for the Navigable Channel, based on the available and historical bathymetric data. The tidal amplitude a was considered equal to the average of the observations and the mean depth h was set equal to the local depth in Station

B. The factor results γ =1.1. According to Dronkers (1998), it denotes an overall prevailing of light flood dominance condition, furtherly confirming previous analysis.

In Figure 13 the results of the harmonic analysis of the signal acquired in Station *B* are displayed, i.e. the amplitude and frequency of the main tidal constituents. Table 1 lists the constituents' phase. The semidiurnal *M2* constituent is the dominant component of the tidal regime observed at the Mar Piccolo basin, with an amplitude value of 0.044 m. Further main constituents are *S2*, *N2*, *L2* and *K1*. As already evidenced from the FFT analysis, in the basin the tidal movement is the main driving force for the horizontal water flow.

Applying Eq.2 for the study case and referring to data of Figure 13 and Table 1, the form number *F* results equal to 0.726, which corresponds to a semidiurnal regime, as expected.

The primary source of asymmetry in the Mar Piccolo, governed by a semidiurnal tidal regime, is the interaction of the principal lunar semidiurnal tide *M2* with its first overtide, the lunar quarter diurnal *M4,* as also reported in similar case studies (Aubrey and Speer, 1985; van de Kreeke and Robaczemska, 1993).

Finally, referring to phase values in Table 1, the calculated phase difference $2\theta_{M2} - \theta_{M4}$ by Aubrey and Speer (1985) results equal to about 145°, furtherly confirming the flood dominant conditions already highlighted.

3.4 Tide and currents correlation

The adopted approach, based on an analysis in time and frequency domains, proved that the flow current along the Navigable Channel has a vertical structure connected and varying with the tide phase, specifically characterized by a cyclic trend. As well, on the seasonal period, the Mar Piccolo basin resulted dominated by a semidiurnal tide regime, with a predominance of flood currents, above all in deeper layers. To extrapolate these results and trying to provide a practical prediction scenario, the possible correlations between the longitudinal currents in the Channel and the tidal records were investigated. Firstly, in qualitative terms, the vertical profiles of the longitudinal current velocity *v*, assessed at Station *A*, were analysed at four selected phases for each tidal cycle: tide crest, passage from crest to trough, tide trough and passage from trough to crest. For the sake of brevity, only four profiles are shown (Figs. 14a÷d), referring to successive steps in sequence, chosen as representative of the whole period. Analogous behaviours in fact were noted during all the other tide cycles.

Figure 14a shows the vertical trend of the longitudinal current velocity corresponding to the passage from trough to crest (15.11.2015, hour 23:00). In this case, the flow is directed towards the Mar Grande near the surface and reverses at about 3m depth, being directed towards the Mar Piccolo from this depth to the bottom. Figure 14b displays the vertical profile of *v* during the crest (16.11.2015 hour 02:00), when the assessed longitudinal velocities are all positive values, varying in the range 0.1m/s ÷ 0.25m/s. In this case, the longitudinal current is directed toward the Mar Piccolo basin at all depths. Figure 14c exhibits the vertical profile of the *v* longitudinal velocities during the passage from tide crest to tide trough (16.11.2015, hours 05:00). It is characterized by negative values in the most superficial layer, meaning the presence of an outflow directed towards the Mar Grande, while positive values are observed at greater depths, starting from *z*=-5m depth up to the bottom. During the passage of the tide trough (16.11.2015, hours 08:00) shown in Figure 14d, the measured *v* velocities are negative along the whole depth, with values in the range -0.08m/s ÷ -0.40m/s. This case is thus characterized by an outflow towards the Mar Grande.

It is worth observing the following. The transit of both tide crest and tide trough rapidly involves the whole water depth, inducing a mass transport such as a progressive wave (inflow towards the Mar Piccolo for the crest case and outflow from the Mar Piccolo for the trough case). The passage from tide crest to trough (Fig. 14d) highlights that the approaching trough induces a general reduction of the *v* positive velocities generated during the previous crest transit and causes a

flow reversing near the surface, with v values becoming negative. In the passage from trough to crest, the presence of superficial positive v values due to the approaching crest was expected, together with negative values generated by the previous trough transit at greater depths. On the contrary, the vertical profile of v still shows negative values in a thin superficial layer and positive values at greater depths (Fig. 14a). This trend should be interpreted also taking into account that in the Navigable Channel water temperature and salinity are not uniform along the water column and that a thermohaline gradient occurs. The annual mean salinity distribution investigated in previous researches (Umgiesser, 2007; De Pascalis et al., 2015) showed that freshwater inflows in the Mar Piccolo, from both subaerial watercourses and submarine springs, create an increasing gradient between the Mar Piccolo and the Mar Grande. Moreover, they stated that freshwater stays on the surface layer, while near the bottom salinity is increased of about 1 PSU in most of the basin. Referring to annual averaged temperature trends, De Pascalis et al. (2015) noted that the morphological and bathymetric differences between the sub-systems influence their thermal inertia and create an increasing temperature gradient going from the open sea to the inner part of the basin. As a consequence, it seems consistent that during the passage from trough to crest (Fig. 14a) the approaching crest conveys toward the Mar Piccolo a more saline and cold flux, i.e. a dense flux which promptly affects the lower part of the channel.

The correlation between tide and currents flowing through the channel was quantitatively investigated in the frequency domain. In fact, also the time series of the longitudinal currents measured at all depths were processed through a spectral analysis, acted by means of the FFT. The amplitude spectrum of the recorded tide level data in the Navigable Channel was therefore compared with each amplitude spectrum of the measured longitudinal current v at all the different water depths. Figure 15 shows these amplitude spectra, obtained for tide (top raw) and for current data at equally spaced depths of 0.5m, starting from z=-1.5m (from second to ninth row).

The two the peaks of amplitude in the spectrum of tide levels, at frequencies corresponding to 12h and 24h respectively already noted in Figure 3a, are also present in the amplitude spectra of the current signals, at all the investigated depths (Figure 15). Moreover, the current amplitudes on both these frequencies slightly decrease from the surface toward the bottom, revealing that the tide effect is stronger in the most superficial layers. Finally, it can be stated that the current flow in the Navigable Channel could also be affected by wind or thermohaline actions, but is undoubtedly dominated by the semidiurnal tide.

It is worth noting that if changes in the configuration do not occur, it is possible to extrapolate patterns of flux behaviour useful for prediction. The observed correlation between tides and currents in the Channel suggests a well-defined and thus reproducible modification of the vertical flow due to the passage of the tide. On the contrary, if modifications in the configuration occur, extrapolating patterns is possible only if such changes have been captured in the measurement records. In this second case, numerical simulations could conveniently integrate foreseen hydrodynamic scenarios.

4 Discussion

Understanding water circulation within semi enclosed basins and their exchanges with the open sea becomes a prerequisite for sustainable management of these systems. Several studies have addressed the exchange and transport processes between lagoons and open sea, but most detailed process models do not necessarily answer questions at the time and space scales of interest for coastal managers.

Following the methods based on tidal asymmetry (Aubrey and Speer, 1985; Jewell et al., 2012; Di Lorenzo, 1988) or on residual flow determination (Janzen and Wong, 1998; Guyondet and Koutitonsky, 2008), the present study identified some interactions among waves, tides and currents in a narrow channel connecting two semi enclosed basins.

As shown in the previous section, we utilized well-established and classical procedures to extrapolate information and infer typical and recurring trends in the target area, starting from a large amount of measured data. The added value of this approach is recognizable in its simplicity and feasibility, so that it can be easily applied to any costal site. The hot question is that the data set, to which apply these procedures, must respect fundamental requirements, such as temporal

5   length of the acquired signals, acquisition frequencies, absence of gaps in the time series, simultaneous measurements of many parameters in the same location.

With the data approach presented in this paper, we found some indicators able to simply but adequately and quantitatively describe the state and the evolutionary trend of the investigated basin. These indicators can be identified in i) the net flow crossing a connecting channel, ii) the time delay of current peaks between upper and bottom layers, iii) the tidal

10   asymmetry factor. In fact, a basin system characterization can be deduced from these indicators, since they unable us to deduce a link between forcing data (tide) and response data (currents). In this sense, we are in the condition to attempt a forecasting of the response data over short timescales, i.e. time spans that are considerably shorter than the length of the investigated data time series.

5 Conclusions

15   We illustrated a data-driven framework with the goal of documenting the key mechanisms governing the fluxes flowing through coastal semi enclosed basins. Our approach has significance due to the unique high quality / high resolution collected data set, which allowed to identify physical processes and recurring trends on a seasonal period. Further, the used processing methodology was characterized by well-established and classical procedures, which can be easily applied to similar contexts.

20   As a test bed for the approach, we examined and discussed the effect of tide and currents fluxes on the Mar Piccolo basin, using field measurements derived from a fixed ADCP, a wave array and an ultrasonic tide gauge, referring to a seasonal time frame.

Firstly, the tidal signal was processed by the *FFT* algorithm to prove that it was not affected by possible spurious signals, such as vibrations due to its location on a swinging bridge and wave heights contributions. Successively, the currents

25   flowing through the Navigable Channel were time averaged on the reference period and analysed. It was observed that at deeper layers, from the bottom up to 4m depth from the surface the net flow is inflowing, while in the most superficial layer it is directed outward of the basin. This result confirms both previous numerical modelling (De Pascalis et al., 2015) and previous field data analysis (Armenio et al., 2016; De Serio and Mossa, 2016a).

The correlation between currents and tide was inspected initially with a qualitative approach. The comparison of both the

30   phase averaged signals displayed that, for increasing depth from the surface, the tide affects the current with a time delay, generally equal to two-three hours. The hourly vertical profiles of the measured longitudinal currents were deduced. They showed that the transit of both tide crest and tide trough rapidly involves the whole water depth, inducing a mass transport such as a progressive wave (inflow towards the Mar Piccolo for the crest case and outflow from the Mar Piccolo for the trough case). Referring to the intermediate passages, when the trough is approaching, it induces a reduction of the

35   velocities generated during the previous crest transit and causes a flow reversing near the surface (i.e. a superficial outflow). When the crest is approaching, it conveys colder and more saline water coming from the external basin, therefore a dense flux promptly affects the lower part of the channel.

The correlation in quantitative terms was found by means of a spectral analysis of both tide and current signals. In fact, two peaks of amplitude in the current spectrum at all the investigated depths, were observed, corresponding to the

frequency peaks of the tide amplitude spectrum (i.e. 12 hour and 24 hour, respectively), also proving that the Mar Piccolo is a semidiurnal tide dominated basin.

Different approaches were applied to investigate on the spatial and temporal tidal asymmetry. The ratio between peaks of ebb currents and peaks of flood currents provided that ebb dominance occurs at surface layer and flood dominance at bottom. Furthermore, at surface layer, the ebb current duration prevails on the flood current duration. Also the tidal asymmetry factor was computed, confirming the flood dominance condition. Finally, the harmonic analysis on the tidal constituents showed that in the target site the principal tidal constituent is *M2*. The phase and amplitude relationships between the *M2* and *M4* constituents again proved a flood dominant condition.

We concluded that even if our results have the limitation to be site-specific, in any way some indicators able to adequately and quantitatively describe the state and the evolutionary trend of any basin are provided. Thus they should be useful for practical predictions in analogous circumstances, when cyclic hydrodynamic trends are expected to recur. Moreover, the adopted methodology is independent from the target site and is applicable to many different settings. Therefore, the application presented in this study can be useful for the practitioners to assess the utility of in situ measurements of high quality, beyond or in conjunction with modelling methodologies.

The increasing availability of more high quality measurements, such as water quality data, seems to promise a more complete understanding of coastal fluxes, which is a topic of future research.

References

Armenio, E., Ben Meftah, M., Bruno, MF., De Padova, D., De Pascalis, F., De Serio, F., Di Bernardino, A., Mossa, M., Leuzzi, G. and Monti, P.: Semi enclosed basin monitoring and analysis of meteo, wave, tide and current data, Proc. IEEE Conference on Environmental, Energy and Structural Monitoring Systems. Bari, Italy, 13-14 June, 2016.

Aubrey, D.G. and Speer, P.E.: A study of non-linear tidal propagation in shallow inlet/estuarine systems, Part I: Observations, J. Estuarine Coastal and Shelf Science, 21, 185-205, 1985.

Boon, J. D. and Byrne R. J.: On basin hypsometry and the morphodynamic response of coastal inlet systems, J. Mar. Geol., 40, 27–48, 1981.

Boon, J.D.: Temporal variation of shallow water tides in basin inlet system. In: Audrey D.G and Weishar, J. (Eds.) Springer Verlag, New York, 1988.

Byun, D.S. and Cho, Y.K.: Double peak-flood current asymmetry in a shallow-water-constituent dominated embayment with a macro-tidal flat, Geophys. Res. Lett., 33, L16613, 2006.

Benque´, J.P., Cunge, J.A., Feuillet, J., Hauguel, A. and Holly, F.M. Jr.: New method for tidal current computation. ASCE J. Wat., Port, Coas. and Oce. Div. 108, 396–417, 1982.

Brown, J. M. and Davies, A. G.: Flood/ebb tidal dominance in an estuary: sediment transport and morphology. Proc. 5th IAHR International Symposium on 'River, coastal and estuarine morphodynamics', University of Twente, Enschede, The Netherlands, pp. 17-21, 2007.

De Serio, F., Malcangio, D. and Mossa, M.: Circulation in a southern Italy coastal basin: modelling and field measurement, J. Con. Shelf. Res., vol. 27, 779–797, 2007.

De Serio, F. and Mossa, M.: Streamwise velocity profiles in coastal currents, J. Env. Fluid. Mec., 14 (4), 895-918, 2014.

De Serio, F. and Mossa, M.: Analysis of mean velocity and turbulence measurements with ADCPs. J. Adv. Water Res., 81, 172–185, 2015.

De Serio, F., and Mossa, D.: Environmental monitoring in the Mar Grande basin (Ionian Sea, Southern Italy), J. Env. Sci. and Poll. Res., 23 (13), 12662-12674, 2016a.

De Serio, F. and Mossa, M.: Assessment of hydrodynamics, biochemical parameters and eddy diffusivity in a semi-enclosed Ionian basin, J. Deep-Sea Res. II, 2016b. doi: 10.1016/j.dsr2.2016.04.001.

De Pascalis, F., Petrizzo, A., Ghezzo, M., Lorenzetti, G., Manfè, G., Alabiso, G. and Zaggia, L.: Estuarine circulation in the Taranto Seas, J.Env. Sci. and Poll. Res., 9, 2015.

Di Lorenzo, J.L.: The overtide and filtering response of small inlet/bay systems. In: Aubrey, D.G., Weishar, L. (Eds.), Hydrodynamics and Sediment Dynamics of Tidal Inlets.: Lecture Notes on Coastal and Estuarine Studies. Springer-Verlag New York, Inc, New York, 24–53, 1988.

Dronkers, J.: Tidal asymmetry and estuarine morphology. Netherlands, J. Sea Res., 20(2), 117-131, 1986.

Dronkers, J.: Morphodynamics of the Dutch Delta, In: J. Dronkers, M.B.A.M. Scheffers (eds.) Physics of Estuaries and Coastal Seas, Balkema, Rotterdam, 297-304, 1998.

Fortunato, A.B. and Oliveira, A.: Promoting ebb dominance in coastal lagoons. In: Smith, J.M. (Ed.), 29th International Coastal Engineering Conference, 19–24 September 2004. World Scientific Publishing Co., Lisbon, Portugal, pp. 1173–1185, 2004.

Friedrichs, C.T. and Aubrey, D.G.: Non-linear tidal distortion in shallow well-mixed estuaries: a synthesis, J. Estuar. Coastal and Shelf Sci., 27, 521-545, 1988.

Godin, G.: The Analysis of Tides, University of Toronto, Press, Toronto, 264, 1972.

Le Provost, C.: Generation of overtides and compound tides (review). In: Parker, B.B. (Ed.), Tidal Hydrodynamics. John Wiley & Sons, Inc., New York, pp. 269–295, 1991.

Guyondet, T. and Koutitonsky, V.G.: Tidal and residual circulations in coupled restricted and leaky lagoons, Estuarine, Coastal and Shelf Science, 77, pp. 396-408, 2008.

Moore, R.D., Wolf, J., Souza, A.J. and Flint, S.S.: Morphological evolution of the Dee Estuary, Eastern Irish Sea, UK: a tidal asymmetry approach. J. Geomorph., 103, 588–596, 2009.

Nidzieko, N. J.: Tidal asymmetry in estuaries with mixed semidiurnal/diurnal tides. J. Geoph. Res.: Oceans, 115(C8), 2010.

Janzen, C.D. and Wong, K.C.: On the low-frequency transport processes in a shallow coastal lagoon. Estuaries 21, pp. 754-766, 1988.

Jewell, S.A., Walker, D.J. and Fortunato, A.B.: Tidal asymmetry in a coastal lagoon subject to a mixed tidal regime. Geomorphology, 171-180, 2012.

Pawlowicz, R., B. Beardsley, and Lentz, S.: Classical tidal harmonic analysis including error estimates in MATLAB using T_TIDE, Comput. Geosci., 28, 929– 937; 2002.

Pugh, D.T.: Tides, surges and mean sea level. John Wiley and Sons Ltd., Chichester, UK, 472 pp., 1987.

Reeve, D. E., Karunarathna, H., Pan, S., Horrillo-Caraballo, JM., Różyński, G. and Ranasinghe, R.: Data-driven and hybrid coastal morphological prediction methods for mesoscale forecasting, J. Geomorph. 256, 49–67, 2016.

Samaras, AG., Gaeta, MG., Miquel, AM. and Archetti, R.: High-resolution wave and hydrodynamics modelling in coastal areas: operational applications for coastal planning, decision support and assessment, Nat. Hazards Earth Syst. Sci., 16, 1499–1518, 2016.

Sauvageta, P., Davida, E. and Soaresb, C.G.: Modelling tidal currents on the coast of Portugal, J. Coastal Eng., 40, 393-409, 2000.

Scroccaro, I., Matarrese, R. and Umgiesser, G.: Application of a finite element model to the Taranto Sea. J.Chem. Ecol., 20, 205–224. supplement 1, 2004.

Speer, P.E. and Aubrey, D.G.: A study of non-linear tidal propagation in shallow inlet/estuarine systems. Part II: Theory. Estuarine, J.Coas. and Shelf Sci. 21, 207–224, 1985.

Townend, I., Wright, A., and Price, D.: An investigation of the gross properties of UK estuaries, In: Modelling Estuary Morphology and Process, Report Prepared by the EMPHASYS consortium for the Estuaries Research Programme Phase 1, MAFF Project FD1401, 2000.

Townend, I.: An examination of empirical stability relationships for UK estuaries, J. Coastal Research, 21, 1042 – 1053, 2005.

Umgiesser, G., Scroccaro I. and Alabiso G.: Mass exchange mechanisms in the Taranto Sea. Transitional Waters Bulletin I(2): 59–71, 2007.

Van de Kreeke, J.: Hydrodynamics of Tidal Inlets, Hydrodynamic and sediment dynamic od tidal inlet, Audrey D.G and Weishar, J. (Eds.) Springer Verlag New York, 1-23, 1988.

Westerink, J.J., Connor, J.J. and Stolzenbach, K.D.: A frequency-time domain finite element model for tidal circulation based on the least-squares harmonic analysis method. International J.J Numerical Methods in Fluids 8, 813–843, 1988.

Tidal constituents	Q1	O1	K1	J1	N2	M2	L2	S2	M3	M4	S4	M6	M8
Phase (θ) (degrees)	348.4	21.8	152.0	258.4	152.0	162.9	270.0	347.8	243.6	180.9	301.3	203.2	264.7
SNR	0.064	0.7	4.1	0.45	2.8	17	3.4	2.3	2.1	1.9	0.85	0.64	0.06

Table 1: Phase and signal-to-noise ratio (SNR) of tidal constituent.

a)

b)

Figure 1: Map of the study area of Mar Piccolo in the south of Italy, b) enlargement on the position of station A and station B in the Navigable Channel. Source Google Earth.
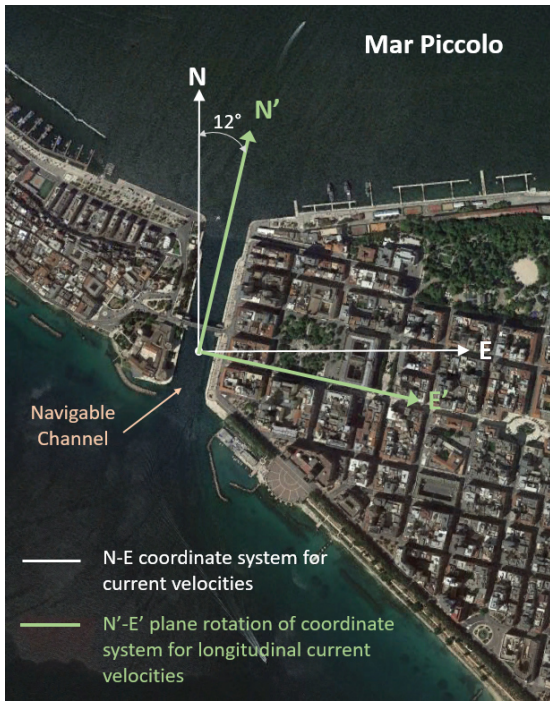
Figure 2: Initial coordinate system adopted for current velocities (white) and plane rotation of the coordinate system for longitudinal current velocities (green)

5
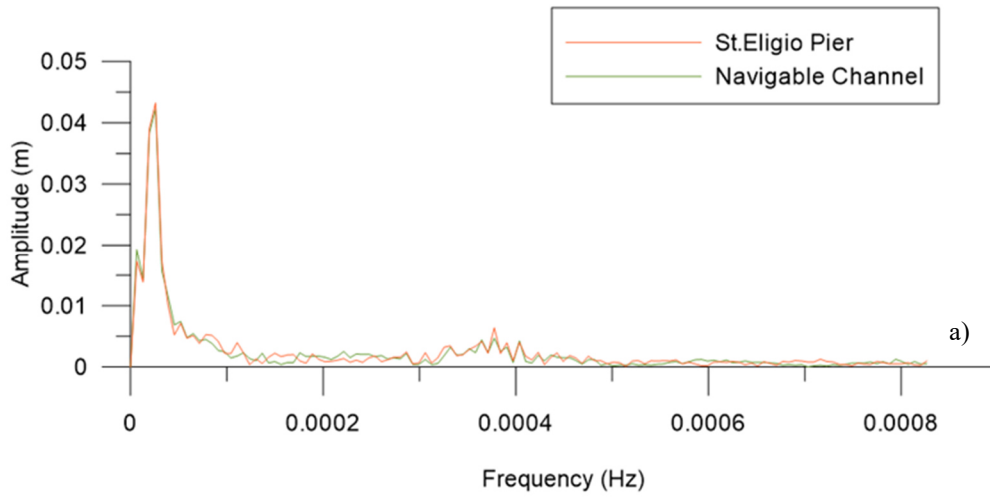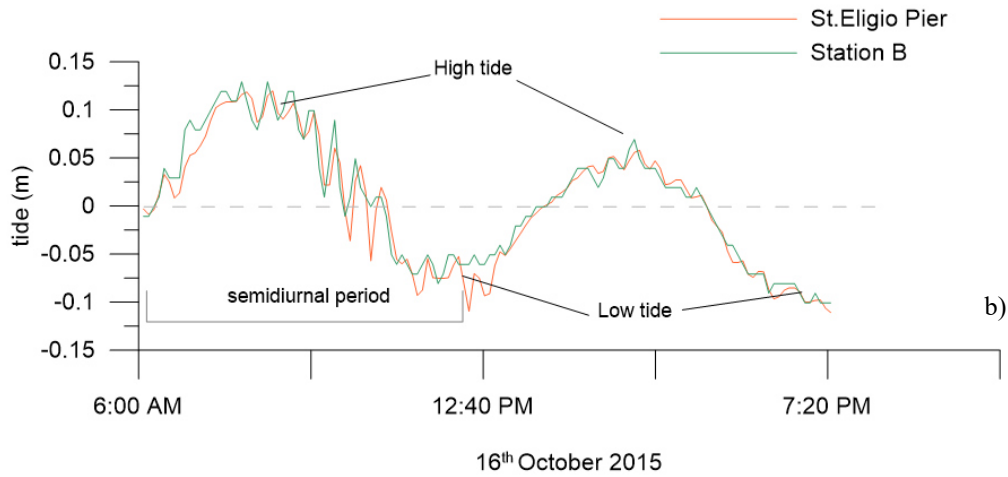
Figure 3: Comparison between a) the amplitude spectra of tidal data recorded by Station B and Station St. Eligio; b) the tidal signals measured at Station B and Station St. Eligio during the extreme meteorological event, on 16.10.2015.

5

c)
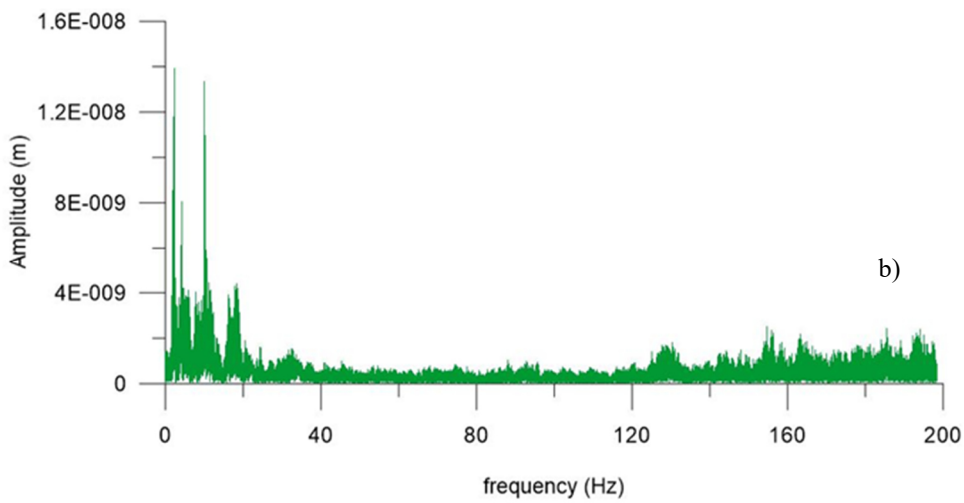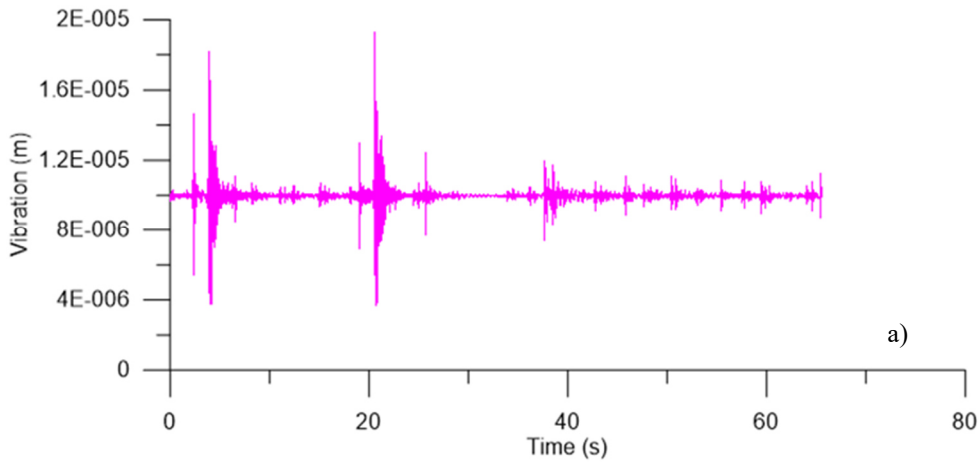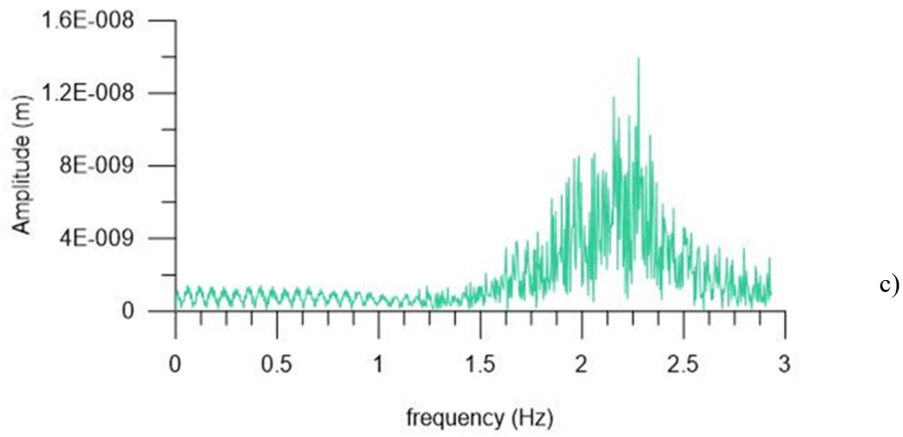
Figure 4: a) Time series of bridge vibrations; b) Amplitude spectrum of bridge vibration; c) Enlargement of the amplitude spectrum in the frequency range 0 ÷ 3.0 Hz.
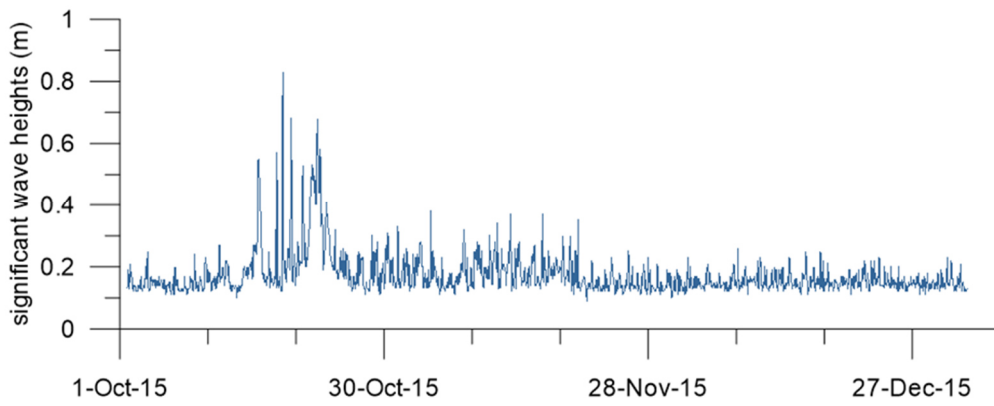
5

Figure 5: Time series of the significant wave heights *Hs* for the investigated period.

18
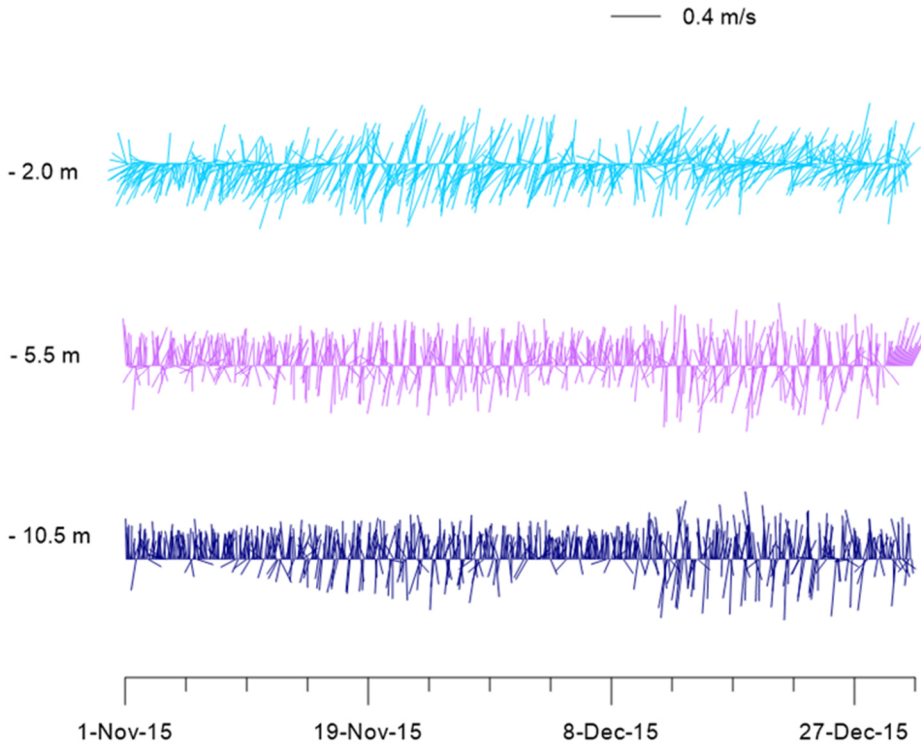
Figure 6: Stick plot of the current vectors at depths z=-2.0 m, z=-5.5 m and z=-0.5m from surface.
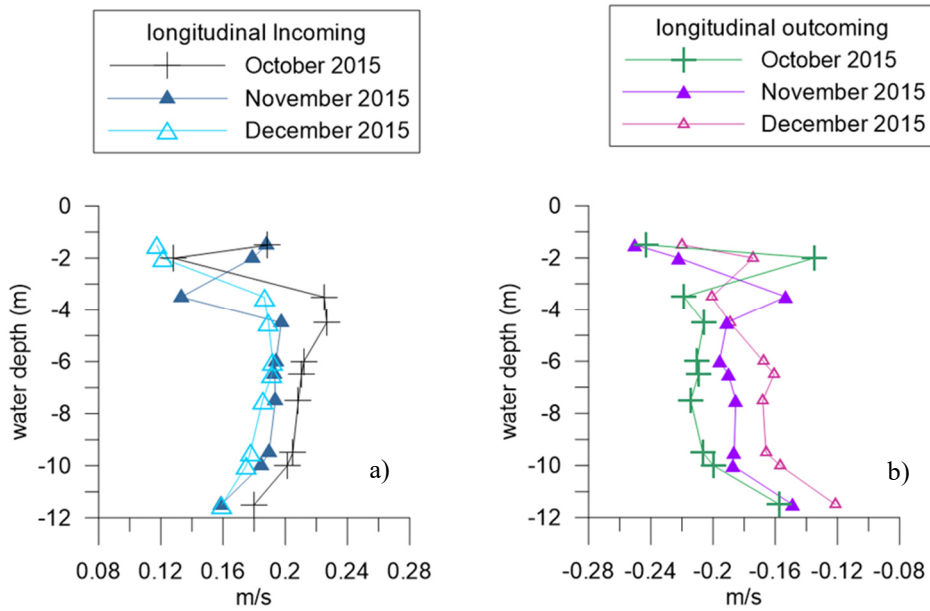
Figure 7: Monthly-averaged values of the longitudinal components of a) the incoming flow and b) the outcoming flow.
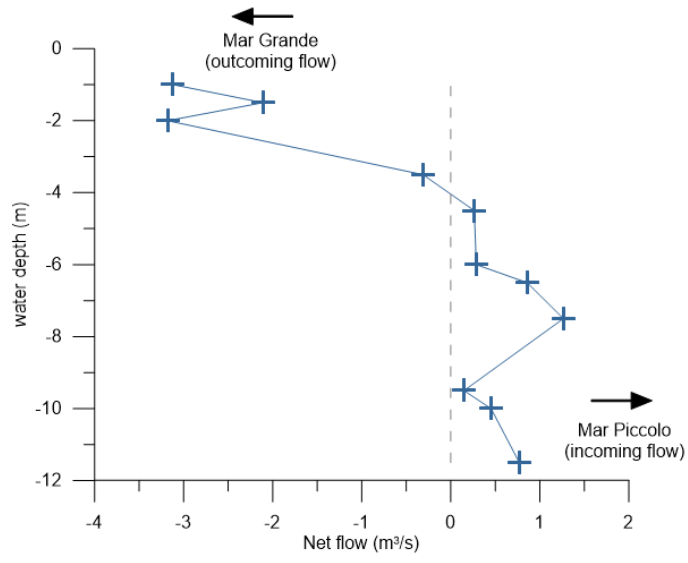
Figure 8: Net flow across the Navigable Channel in the reference period.
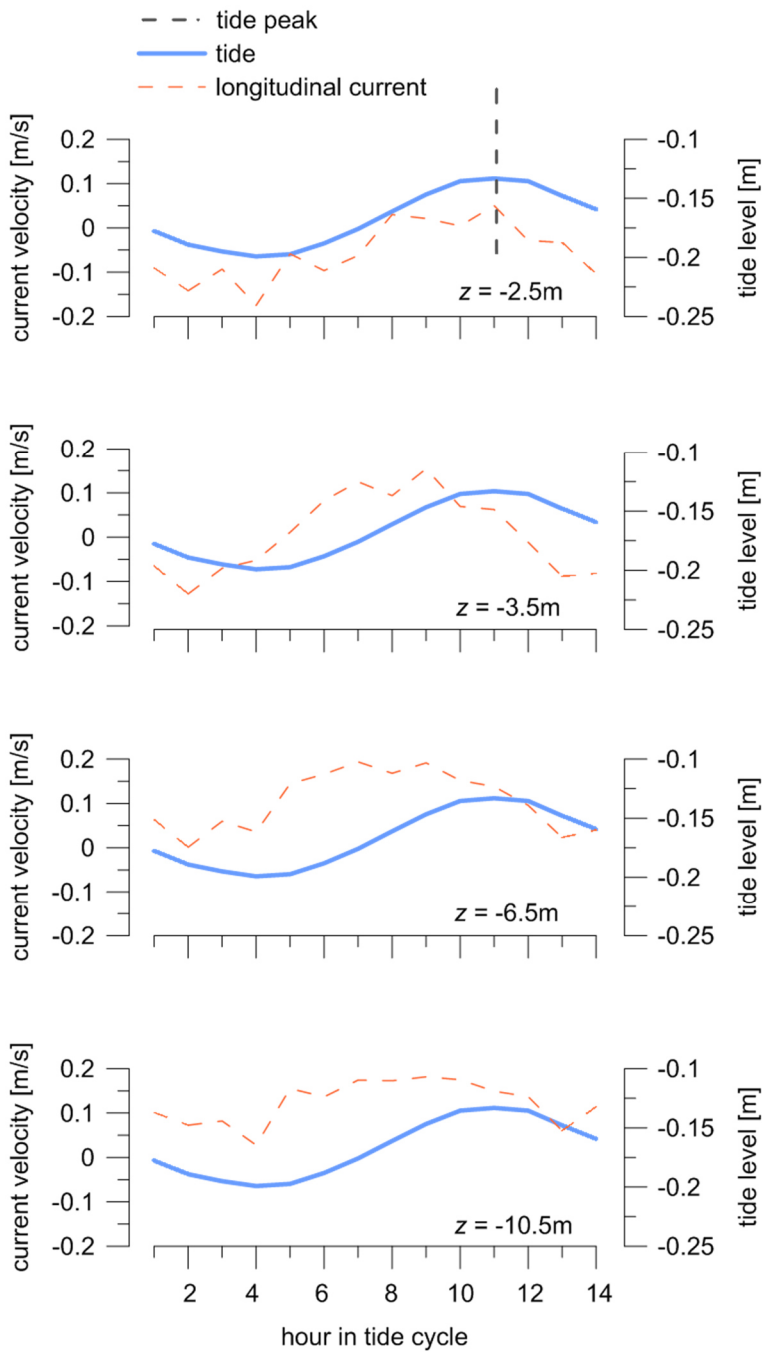
Figure 9: Phase-averaged tidal elevations (blue line) and longitudinal current-velocities (dotted orange line) at some selected depths z.

5

10
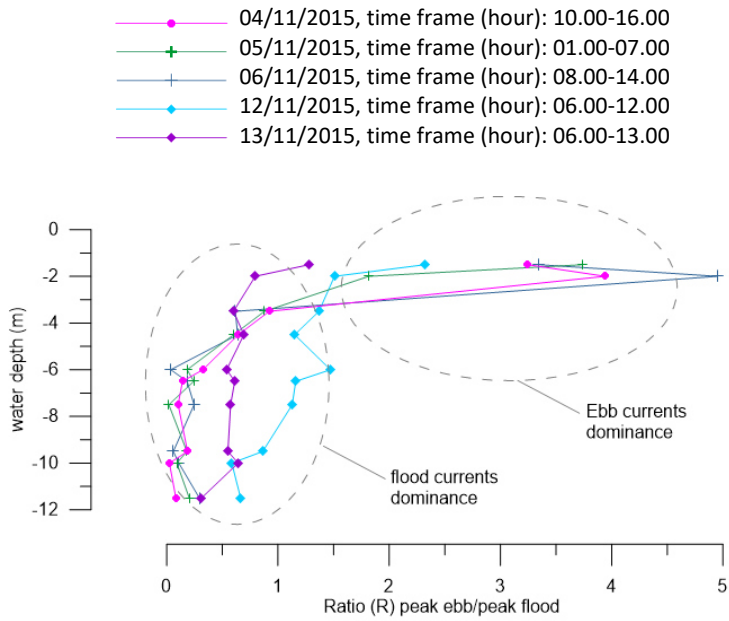
Figure 10: Ratio *R* for different water depth for five selected time frames.
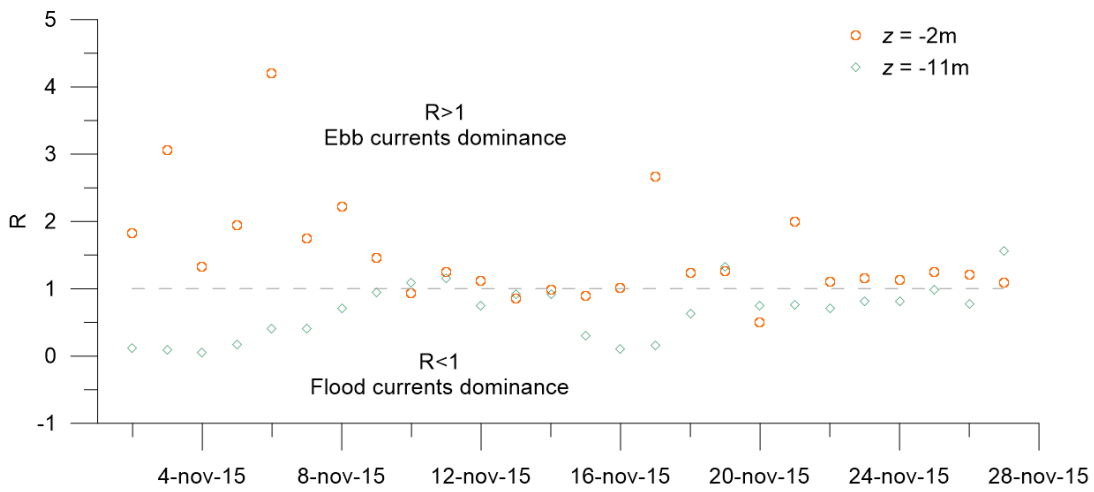
5

Figure 11: Monthly variability of the ratio R for November 2015, near the surface and near the bottom.
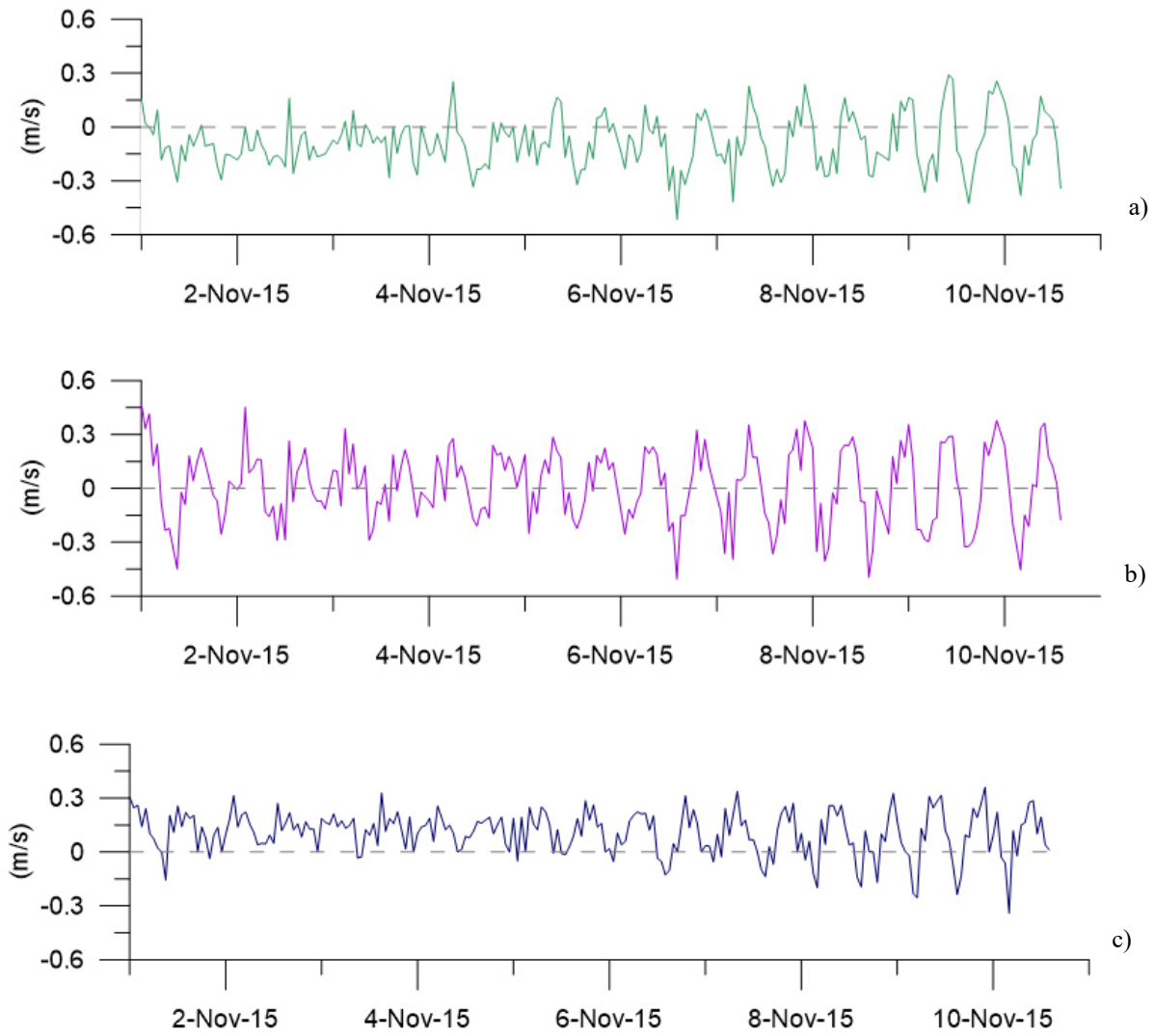
Figure 12: Duration of floods and ebbs at a) $z=-2.0$ **m, b)** $z=-6.0$ **m and c)** $z=-10.5$**m. Time window from 01.11.205 hour 00:00 a.m. to 10.11.2015 hour 09:00 p.m.**

5
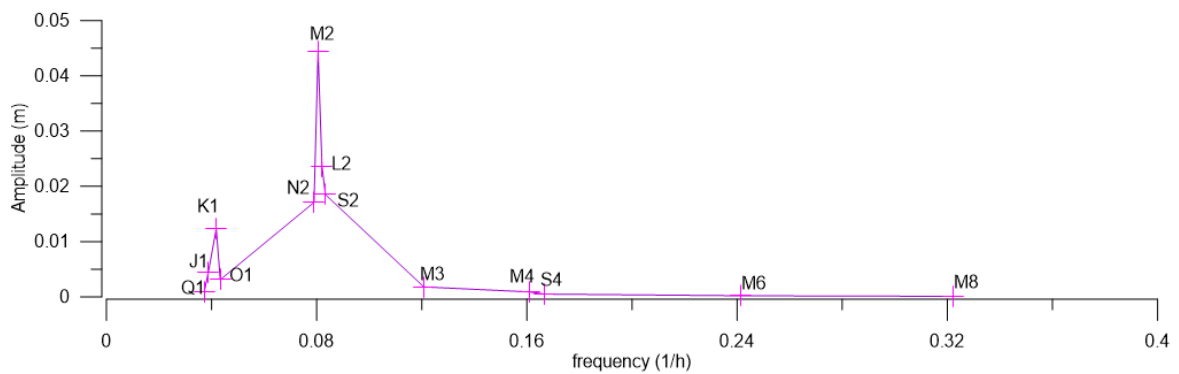
Figure 13. Summary of the harmonic analysis results for tides recorded at Station B.

23

a — 15.11.2015 - hour 23:00 [trough-crest]

b — 16.11.2015 - hour 2:00 [crest]

c — 16.11.2015 - hour 5:00 [crest-trough]

d — 16.11.2015 - hour 8:00 [trough]
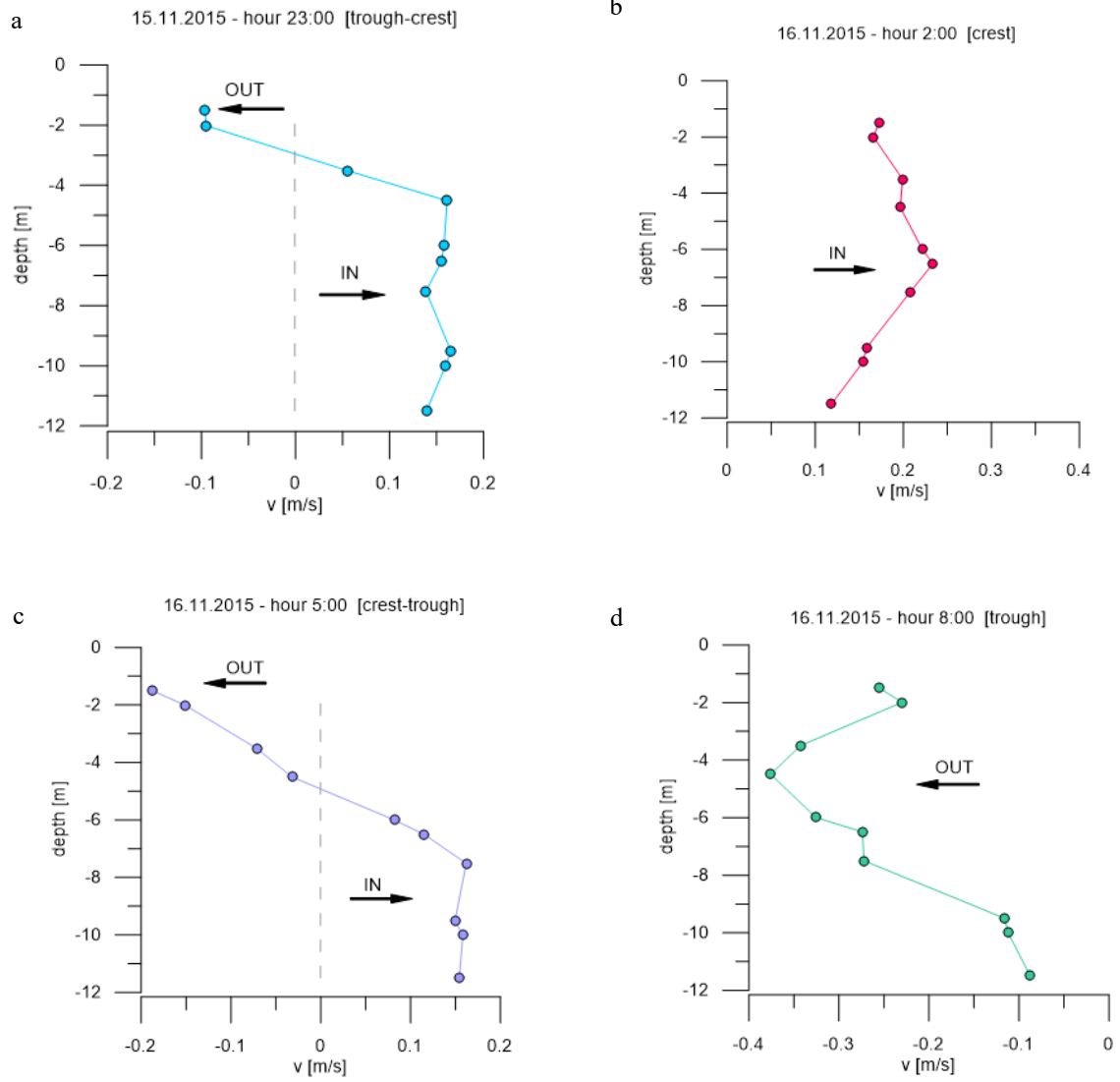
5   **Figure 14: Vertical profiles of the longitudinal current velocity v at four different instant times, along a tidal cycle.**
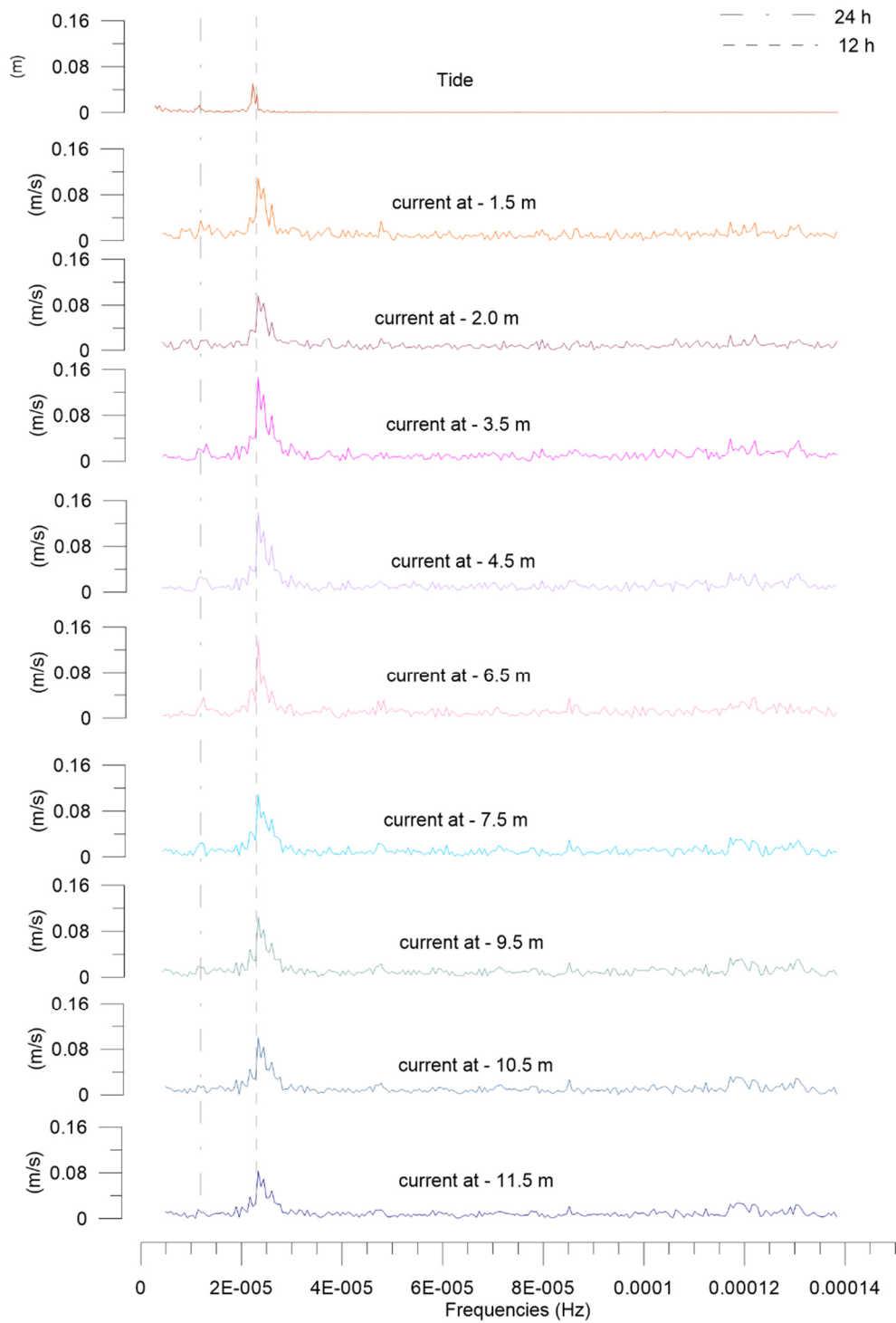
Figure 15: Amplitude spectrum of tide data (m) at Station B and of the longitudinal current velocity at Station A (m/s) for different water depths from surface.

5